Essential Readings in Light Metals: Cast Shop for Aluminum Production.
Edited by John F. Grandfield and Dmitry G. Eskin.

Light Metals — From *Light Metals 1992*, Euel R. Cutshall, Editor

ON THE KINETICS OF REMOVAL OF SODIUM FROM ALUMINUM AND ALUMINUM-MAGNESIUM ALLOYS

B.Kulunk and R.Guthrie
McGill Metals Processing Centre
Department of Mining and Metallurgical Engineering
McGill University, Montreal, H3A 2A7, PQ, Canada

ABSTRACT

An experimental study was undertaken to determine the effects of chlorine gas volume fraction (0-25%) in the fluxing gas, fluxing gas flowrate (7.79-27-07 cc/sec @NTP) on the rate of removal of sodium from aluminum and aluminum-1 wt% magnesium alloys. For this purpose, fluxing gas was introduced into a 7.5 kg melt by an upward facing nozzle and bubble frequency was measured during the course of the experiments. The number and size distribution of chloride particles and/or droplets that were generated by the chlorination of the melt were measured by using the LIMCA (**L**iquid **M**etal **C**leanliness **A**nalyzer). This data was used to calculate the mass transfer coefficients for the chloride droplets.

INTRODUCTION:

Sodium in aluminum is an undesirable element as it causes hot cracking during hot-rolling of aluminum-magnesium alloys. Several studies have been undertaken to investigate the removal of sodium from aluminum and aluminum-magnesium alloys.

Patak et al.[1] investigated the effect of holding, stirring, inert and reactive gas bubbling at various temperatures on the kinetics of sodium removal from commercially pure aluminum melts. A boron-nitride nozzle was used to create a high velocity, pencil thin, jet producing a fine dispersion of gas bubbles of approximately 0.001 m diameter within the melt. The size of these bubbles was estimated on the basis of water model experiments. They showed that by inert gas purging, about 92% of the sodium was removed from the melt by evaporation from the surface. Only 8% of the sodium was carried out of the melt by the purge gas bubbles.

In the case of reactive gas injection, 5 vol% of Cl_2, CF_2Cl_2, CF_4Cl_2 and SF_6 were used respectively in conjunction with nitrogen. Although it is difficult to compare their results since experimental conditions were not equivalent, it was apparent that the highest rates of removal were obtained when using reactive gas fluxing with stirring. The authors also hinted that the use of $MgCl_2$ as a reactive agent would enhance the rate of removal of sodium from aluminum melts. However, no experimental results as to the degree to which $MgCl_2$ would be effective were presented.

Engh et al.[2] studied the removal of sodium from Al-5 wt% Mg alloys by various methods: i) mechanical stirring with an impeller, ii) an impeller+$MgCl_2$ top salt addition, iii) an impeller and inert gas(Ar) with or without top salt addition and iv) Ar-2 vol% Cl_2 mixture with impeller stirring. They argued that provided the surface area of contact between bubbles and melt was sufficient, sodium removal would be governed by the stoichiometry of the reaction between dissolved sodium and chlorine gas. Similarly, they postulated that should the net contact area be insufficient, then the rate of sodium removal would be controlled by mass transfer of dissolved sodium in the molten metal phase. In their experiments they demonstrated that they were able to achieve sufficient contact area for the former condition to apply. Bubble sizes were determined by conducting water model experiments. No direct measurements of bubble sizes were carried out under actual experimental conditions. These authors clearly showed the positive effect of $MgCl_2$ top salt addition on the rate of removal of sodium.

Based on their water model tests, Engh et al. postulated that gas bubbles rising through the molten aluminum would suppress the vortex generated through the rotation of their impeller. They argued that this, in turn, would decrease the positive effect of $MgCl_2$ droplets generated by vortex formation. However, they were not able to quantify the number and size distribution of these droplets to confirm their hypothesis.

Purpose of the Present Study:

The purpose of the present study has been to determine each factor contributing to the kinetics of removal of sodium from aluminum and aluminum-magnesium alloys using gas chlorination. In the following, thermodynamic and kinetic considerations are presented, together with a description of experimental equipment, procedures and results.

I.THEORY

I.1 Thermodynamics of Chlorination:

In order to determine thermodynamically likely reaction products and corresponding magnitudes during chlorination of aluminum and aluminum-1 wt% magnesium alloys containing minute amounts of sodium, use was made of the F*A*C*T program available in McGill University's Main Frame Computer.

Based on our experimental procedures, a 7.5 kg charge of pure aluminum, or an aluminum-1 wt% magnesium alloy,

was taken to represent the liquid phase. This liquid phase was assumed to come into equilibrium with a gas phase in the form of gas bubbles of argon and chlorine mixtures of various composition. The results of such thermodynamic calculations for Al-Cl_2, Al-Na-Cl_2 and Al-Mg-Na-Cl_2 systems are now presented.

I.1.a Aluminum-Chlorine system:

Figure 1. shows the mole fraction of gaseous reaction products as a function of chlorine concentration in the gas bubbles at 730 °C. The mole fraction of argon was not included in this figure. When gas bubbles containing 100 % chlorine were utilised, $AlCl_3$ was the most favoured gas species of the reaction products to form. This was followed by $AlCl_2$, $AlCl_6$ and AlCl in decreasing order. There were also Cl and Cl_2 present in the products. However, these were at least 10 to 16 orders of magnitude smaller and are therefore not included in the graphs. As the chlorine concentration in the gas bubbles decreased, equilibrium conditions shifted, such that below 10 % Cl2, the most favoured gas species to form was $AlCl_2$, followed by $AlCl_3$, AlCl, Al_2Cl_6. Calculations also showed that below 30 % Cl_2, formation of AlCl was more favourable thermodynamically, than Al_2Cl_6.

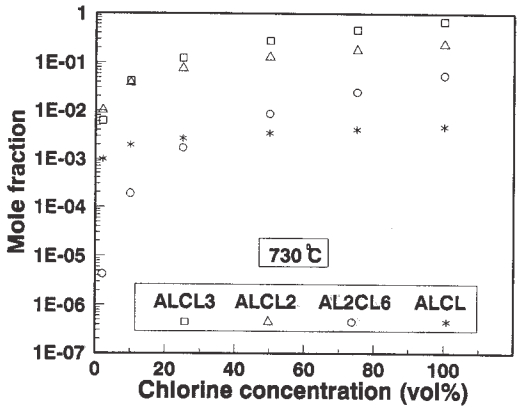

Figure 1. Mole fraction of gaseous product species as a function of Cl_2 concentration at 730 °C

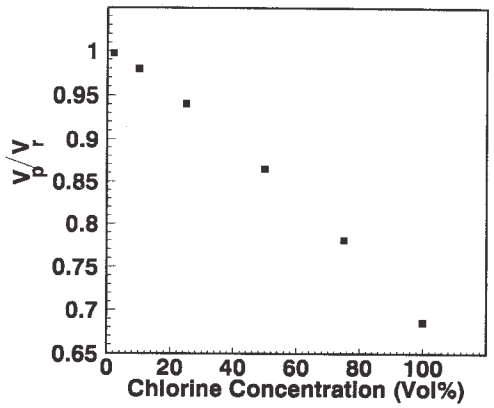

Figure 2. Ratio of the volume of the gaseous reactant species to that of gaseous product species as a function of Cl_2 concentration at 730 °C

Figure 2. shows the ratio of the volume of the gaseous reactant species to that of gaseous product species as a function of Cl_2 concentration at 730 °C. As seen, the volume of the product gas phase decreased with increase in Cl_2 concentration due to decrease in the total number of moles following reaction.

I.1.b. Aluminum-Sodium-Chlorine System:

The activity coefficients of sodium used in calculations for this system were taken from the data of Mitchell and Samis [3]. In these calculations, the activity coefficient of aluminum was taken to be unity.

Figure 3. shows the mole fraction of gaseous product species as a function of chlorine concentration at 730 °C. Under equilibrium conditions, the most favoured gas species to form was sodium vapour, followed by NaCl, Na_2Cl_2, Na_2, AlCl and $AlCl_3$ in decreasing order. The mole fraction of argon was not included in this figure.

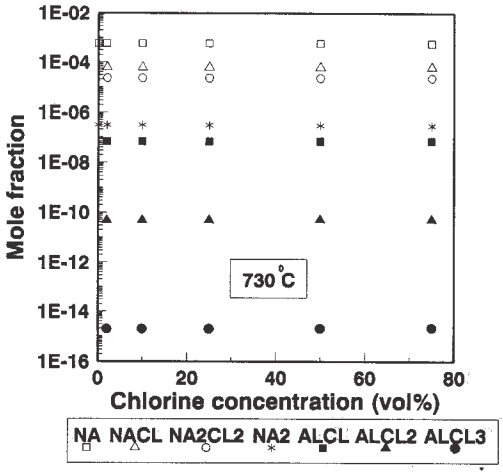

Figure 3. Mole fraction of gaseous product species as a function of Cl_2 concentration at 730 °C.

Calculations showed that solid NaCl was the condensed reaction product. The number of moles of the solid NaCl increased in direct proportion to increase in the chlorine concentration.

I.1.c Aluminum-Magnesium-Sodium-Chlorine System:

In the calculations for this system, in order to take into account the departure from ideal solution behaviour of Al-Mg alloys, a user supplied private solution data file which contained expressions to calculate Excess Gibbs Free Energy of Solution, ΔG^{xs}, at 1000°K was created. The data for this calculation was taken from Selected Values of Thermodynamic Properties of Metals and Alloys compiled by Hultgren et al. [4]. The value of ΔG^{xs} at 1000° K was taken to be:

$$\Delta G^{xs} = -1600 X_{Al} X_{Mg} \quad \text{Calories/mole}$$

In the absence of any experimental data for the Al-Mg-Na ternary system the above data for Al-Mg system, together with the activity coefficients for sodium in Al-Na system, were used in the calculations. Condensed reaction products, $MgCl_2$ and NaCl, were treated as forming an ideal solution.

Figures 4.a and b show mole fraction of gaseous product species as a function of chlorine concentration at 730 ^{0}C. The mole fraction of Ar was not included in these figures. As seen Na was the primary gas product. Calculations showed that mole fraction of NaCl and Na_2Cl_2 did not change with change in chlorine concentration, whereas mole fractions of Na and Na_2 decreased only 3 and 6 % respectively in an increase in chlorine concentration from 0 to 75 %.

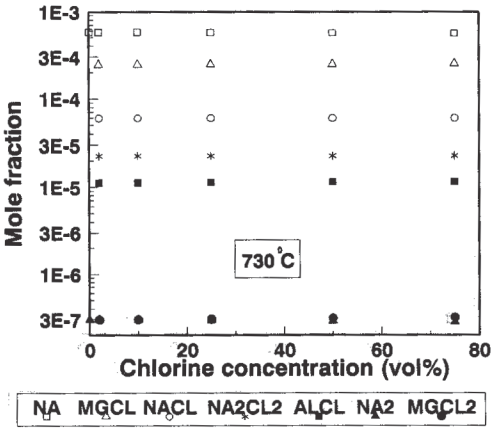

. a .

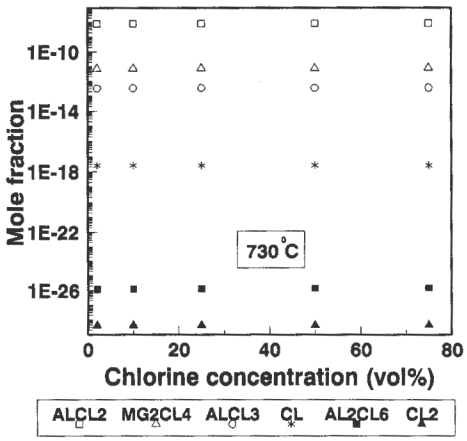

. b .

Figure 4. Mole fraction of gaseous product species as a function of Cl_2 concentration at 730 ^{0}C.

Figure 5. shows the mole fraction of NaCl and $MgCl_2$ in the ideal salt solution. As seen, NaCl was the primary product and the mole fractions of NaCl and $MgCl_2$ practically did not change over the chlorine concentration range considered.

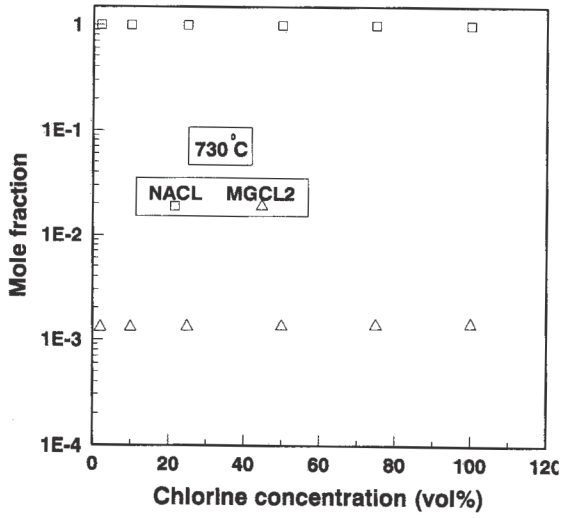

Figure 5. Mole fraction of NaCl and $MgCl_2$ in ideal salt solution at 730 ^{0}C

I.2. Kinetics:

While the preceding thermodynamic calculations are useful in identifying the nature and quantity of reaction products that would be in equilibrium with a given set of reactants under specified conditions of temperature, pressure and concentration, associated kinetics may preclude their formation.

A general schematic description of the chlorination process is shown in Figure 6..

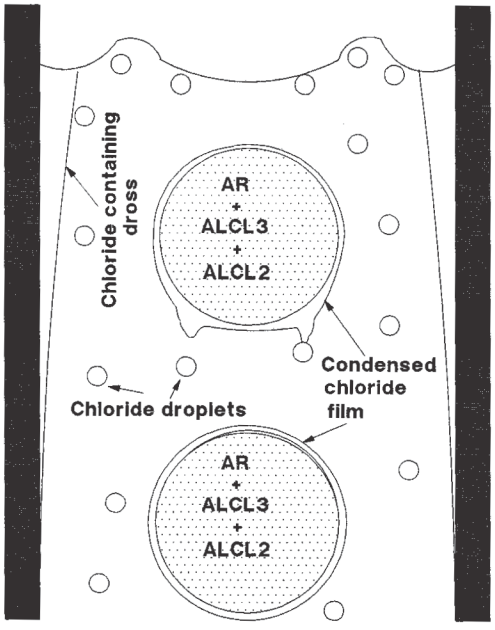

Figure 6. General description of Chlorination Process

There, bubbles, comprising a mixture of chlorine and argon, rising through a bath of liquid aluminum on their way up to the surface, will react with chloride forming elements to form gaseous, liquid or solid reaction products.

These products will depend on the composition and temperature of the melt. In the case of aluminum base aluminum-sodium or aluminum-magnesium-sodium systems, possible reaction products which would be in equilibrium with the reactants were determined, as noted in the thermodynamics section.

If one considers the relative proportions of aluminum, magnesium and small amounts of silicon, manganese and iron invariably present in commercially pure aluminum compared to the minute amounts of sodium within the melt, one would anticipate that kinetic factors will play an important role in determining how reactions will proceed in practice.

In the case of the aluminum-chlorine system, it was seen that on contact with pure aluminum, $AlCl_3$ or $AlCl_2$ would form as a primary gaseous reaction product depending on the volume percent chlorine gas inside the gas bubbles. It can be anticipated that $AlCl_3$ or $AlCl_2$ gas will be the first dominant species to form on initial contact with a base aluminum melt, containing magnesium, iron, manganese, silicon and sodium as solutes owing to aluminum's relatively large mole fraction inside the melt. Thus, despite the fact that some of the above mentioned elements e.g Mg,Mn and Na form chlorides that are thermodynamically more stable than chlorides of aluminum kinetic considerations will dictate that, for short contact times, the latter species will be the predominant form.

Aluminum chlorides will subsequently react with Mg, Fe, Si, Mn, Na to form the chlorides of these elements. Again, due to their larger mole fractions, the dominant reaction products in the case of an aluminum-magnesium alloy will be $MgCl_2$, whereas in commercially pure aluminum, they will be chlorides of Si, Fe or Mn.

Depending on composition and temperature, these intermediate reaction products can form a solid or liquid film over the surfaces of bubbles. It is possible that such films cover the bubbles during their passage through the melt while reacting with minute amounts of sodium. It is also possible that such films can be continuously stripped off from the bubbles by hydrodynamic shear, depending on the physical properties of the film and adhesion characteristics at the melt-salt interface. Such intermediate reaction products, stripped from bubbles, will form liquid droplets or solid particles which, in turn, can be an effective reaction sites for sodium removal.

One can speculate that any remaining unreacted portion of such films will be carried to the melt surface where, again depending on hydrodynamic conditions, then carried towards the crucible wall where they can adhere or be re-entrained into the melt.

Because of its high vapour pressure(0.986 atm @ 730^0 C), sodium can also be eliminated from the melt as a result of evaporation from the melt surface and by evaporation into bubbles.

Consequently, crucible walls , depending on the composition of the crucible material, may also provide a reaction site for the removal of impurities such as sodium, (calcium, lithium, etc).

I.2.1. Kinetic Models for Sodium Removal by Chlorination:

I.2.1.a. Mass Transfer Controlled Sodium Removal:

Referring to Figure 6. and assuming that the removal of sodium from the melt is controlled by transport of sodium in the liquid phase mass transfer boundary, one can construct a mass balance for the bubble stirred reactor system to obtain:

$$-\frac{M\, d\%Na}{100\, m_{Na}} = \frac{k_b\, \rho\, A_b\, [\, \%Na - \%Na_I^{\,b}\,]}{100\, m_{Na}} + \frac{k_0\, \rho\, A_0\, [\, \%Na - \%Na_I^{\,0}\,]}{100\, m_{Na}} + \frac{k_d\, \rho\, A_d\, [\, \%Na - \%Na_I^{\,d}\,]}{100\, m_{Na}} \qquad (1)$$

The term on the left hand side of the equation gives the change in sodium concentration of the melt with time. The first term on the right hand side of the equation represents the rate of sodium removal by reaction at bubble surfaces, the second the rate of sodium removal from the melt due to evaporation from the surface of the melt and, the third, the rate of removal sodium by reaction of sodium with chloride droplets or particles generated as intermediate reaction products.

In this equation interfacial concentrations Na^b_I and Na^d_I are taken to be zero assuming that chemical reactions at bubble surfaces and chloride droplets are fast. For the evaporation term $\%Na_I^0$ was taken zero since the surface of the melt was flushed with argon gas under a closed lid during the experiments.

Upon integration of the above equation one obtains:

$$\frac{\%Na_t}{\%Na_i} = -\exp\left(\frac{k_b\, A_b\, \rho}{M} + \frac{k_d\, A_d\, \rho}{M} + \frac{k_0\, A_0\, \rho}{M}\right) \qquad (2)$$

In the above equation the bracketed terms represent individual rate constants for sodium removal by bubbles, by droplets and by evaporation. The sum of these rate constants represents the overall rate constant. Each rate constant incorporates a liquid phase mass transfer coefficient, the total surface area involved, and terms representing density and mass of the melt.

The purpose of the experimental work was to asses the respective contributions of these modes of sodium removal from the bath.

I.2.1.b. Stoichiometry Controlled Sodium Removal:

In this case it will be assumed that there is sufficient bubble surface area for sodium to react stoichiometrically at the bubbles' surfaces. Any chlorides that form as intermediate reaction products over the bubbles will be assumed to react stoichiometrically with sodium. Evaporation of sodium at the melt surface will be assumed to be controlled by the transport of sodium through liquid phase boundary layer.

A mass balance for this case over the reactor system then gives:

$$-\frac{M\ d\%Na}{100\ m_{Na}\ dt} = 2\ G_{Cl_2} + \frac{G_{ar}\ P_{Na}}{P_{atm} - P_{Na}} + \frac{k_0\ A_0\ \rho}{100\ m_{Na}}\ [\%Na - \%Na_I^0] \quad (3)$$

In this equation, the first term on the right hand side gives the rate of sodium removal through stoichiometric reaction of sodium with chlorine on the bubble surfaces. The second term represents the rate of sodium removal by attaining its equilibrium partial pressure within the bubbles. The last term represents the removal rate of sodium due to evaporation through the melt surface. In this term, the interfacial concentration of sodium was taken to be zero.

The partial pressure of sodium in the denominator of the second term will be dropped because of its much smaller value compared to that of atmosphere. For the partial pressure of sodium in the nominator, the partial pressure of sodium in equilibrium with the bulk sodium concentration was taken:

$$P_{Na} = K f_{Na}\ \%Na \quad (4)$$

With this substitution the above equation becomes:

$$-\frac{M\ d\%Na}{100\ m_{Na}} = 2\ G_{Cl_2} + \frac{G_{ar}\ K f_{Na}\ \%Na}{P_{atm}} + \frac{k_0\ A_0\ \rho}{100\ m_{Na}}\ [\%Na - \%Na_I^0] \quad (5)$$

Following integration, one can show:

$$\frac{A/B + \%Na_t}{A/B + \%Na_i} = e^{-Bt} \quad (6)$$

where A and B represent the following expressions:

$$A = \frac{2\ G_{Cl_2}\ 100\ m_{Na}}{M} \quad (7)$$

$$B = \frac{G_{ar}\ K f_{Na}\ 100\ m_{Na}}{M\ P_{atm}} + \frac{k_0\ A_0\ \rho}{M} \quad (8)$$

II. EXPERIMENTAL SETUP AND PROCEDURE:

II.1 Melt Chlorination Unit:

A schematic of the melt chlorination unit is shown in Figure 7.. A 6.5 KW electrical resistance furnace was used to melt a 7.5 kg charge of aluminum contained in an alumina crucible. The crucible was 0.34 m in length and with an inside diameter of 0.142 m. The top of the crucible was covered with a graphite lid which provided inlets for a gas bubbling lance, impeller, protective argon atmosphere and a sampling ladle. The inlets had screwed-in graphite caps.

After passing the gases through calibrated flowmeters (Gilmont #10 and 12), the high purity chlorine and argon gases were then passed through columns of $CaSO_4$ to remove any moisture. In order to provide adequate mixing, the gases were introduced into a flask containing 0.003 m diameter glass balls. The gas mixture was then injected into the melt through an upward facing quartz nozzle. The inner and outer diameters of the nozzle were 0.004 and 0.006 m respectively.

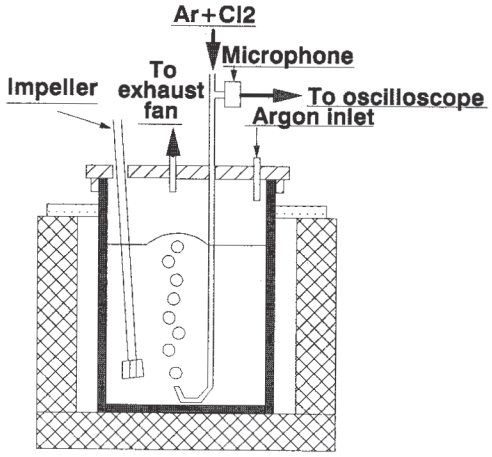

Figure 7. A schematic of the melt chlorination unit

A microphone was inserted into the gas line so as to pick up pressure pulses generated by the release of the bubbles from the tip of the nozzle. The output of the microphone was transmitted to an oscilloscope(Gould 1421) in order to measure the frequency of the bubble formation and thereby, bubble volumes.

A 0.3 m long and 0.0006 m inside diameter polyethylene tubing was used in the gas line between the microphone and the gas mixing unit to minimize the gas chamber volume upstream of the nozzle and therefore to obtain as high a bubble frequency as possible. The rest of the gas line was constructed from 0.064 m inside diameter latex and inner braided tubing.

The melt was stirred with a four blade graphite impeller. The diameter of the impeller was 0.032m. The blades were 0.0007m in thickness and 0.032m in height while the speed of rotation of the impeller was 175 rpm.

The temperature of the melt was measured periodically with a K-type dip-tip thermocouple through a calibrated Omega HH 81 thermometer. The melt temperature was maintained within +/- 3^0 C by controlling the power input to the furnace by an Omega 4001 temperature controller.

As noted, the top of the melt was continuously flushed with high purity argon gas into the gas space beneath the graphite lid during the experiments at 2 l/min (@ NTP) in order to avoid oxidation of the melt as far as possible.

II.1.a Materials:

The aluminum metal that was used in the experiments was kindly donated by Alcan Int. Ltd and was of commercial purity(99.7 wt%).

Magnesium metal that was used to alloy aluminum was kindly donated by Timminco Metals and contained 99.8 wt% magnesium.

Sodium was purchased from Anachemia Inc. and was of technical grade.

II.1.b Experimental Procedure:

In order to introduce sodium to the bath, pure sodium was wrapped in commercially available aluminum foil and dipped into the melt using a bell shaped plunger. The weight of the sodium was adjusted to give 15 ppm dissolved sodium by weight in the melt. Following its addition, the melt was stirred by the impeller for 5 minutes so as to achieve chemical homogeneity. The first sample(approximately 90 gm) was taken using a small ladle and cast into a standard Alcan mould so as to produce a disk shaped sample. Immediately following the first sample, gas was injected into the melt and samples taken periodically. Surface of the disk samples was machined to remove a 0.00015 m metal layer and analyzed using an optical emission quantometer at Alcan's R&D Centre, Kingston. Independent checks on these samples were also done at Alcan's R&D Centre, Arvida. Dross was collected only after gas injection was terminated. The dross was than cooled down to room temperature in small silica crucibles and ground below 200 mesh and submitted for X-ray diffraction analyses.

Table 1. shows the schedule followed for the chlorination experiments during the course of this study. Experiments were carried out for three different gas flowrates(7.79, 16.77, 27.0725 cc/sec @NTP), for four different chlorine gas concentrations(0, 2, 10, 25 vol%) at 730°C.

Table 1. Schedule followed for the chlorination experiments

GAS FLOWRATE (CC/SEC) @NTP	VOL% CL2			
	ALUMINUM		AL-1WT% MG	
	Continuous	Intermittent	Continuous	Intermittent
7.79	0		0	
	2	2	2	2
	10	10	10	10
	25	25	25	25
16.77	0		0	
	10	10	10	10
27.07	0		0	
	10	10	10	10

The purpose of the intermittent tests was to determine the rate constants for intermediate reaction products i.e chloride droplets. In these intermittent tests, a fixed quantity of chlorine($42.42*10^{-3}$ gm-moles) was injected into the melt over a certain period of time together with argon gas. At the end of the period, the chlorine gas supply was cut off and only argon gas was injected into the melt by using a completely separate gas line to avoid contamination by chlorine. Samples were taken starting from the argon only injection period. In these tests, impurity addition was carried out 1 minute prior to the cessation of the chlorine gas supply.

II.2 LIMCA Unit:

In order to determine the size distribution of the chloride droplets i.e intermediate reaction products, a LIMCA(Liquid Metal Cleanliness Analyzer) unit available in the process metallurgy group of the Department of Mining and Metallurgical Engineering at McGill University was used.

II.2.a Principle of Operation:

The operation of the LIMCA is based on the resistive pulse principle of particle size analyses[5]. Figure 8. shows this principle. When particles whose electrical conductivity are less than that of the fluid that they are suspended in pass through an orifice in an insulating vessel, they will replace an amount of the more conductive fluid equal to their volumes. In the presence of an applied current, this replacement of the electrically more conductive fluid volume will register as a temporary increase in the voltage across the orifice.

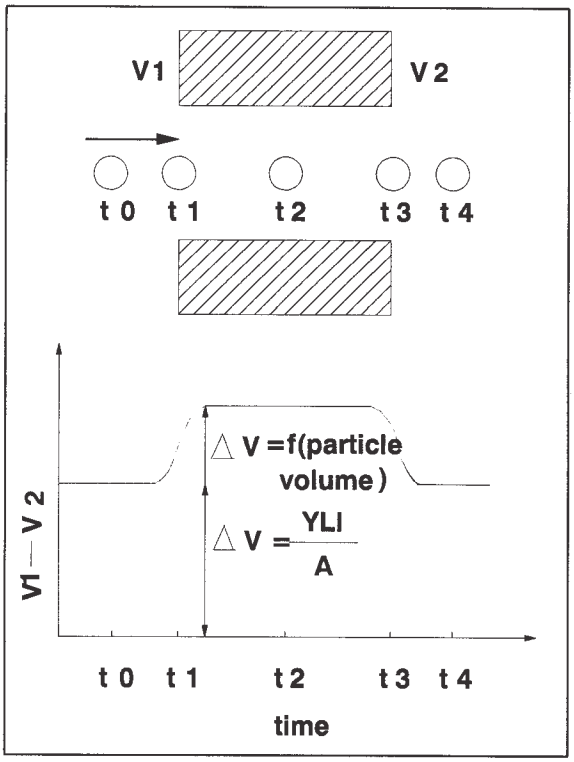

Figure 8. Principle of resistive pulse technique

II.2.b Apparatus:

A schematic of the LIMCA apparatus is shown in Figure 9.. There, by applying vacuum, the liquid metal was sampled through a 300 micron orifice into an insulating sampling cell. The sampling cell was a Kimax brand borosilicate tube which had 0.0254 m diameter and length of 0.25 m. Two mild steel electrodes, one inside the sampling tube and the other inside the melt, were used to maintain a constant current across the orifice.

Voltage signals generated by the passage of the particles through the orifice were monitored and amplified in an oscilloscope and registered in a digital tape recorder. During the playback session, these pulses registered on a digital audio tape were fed back to the oscilloscope. From there, the signals were sent to a pulse sampler which served as a logarithmic amplifier and peak detector. The voltage pulses were than sent to a Multi Channel Analyzer(MCA). There, voltage pulses were mapped linearly according to their magnitude on the 512 channels of the MCA. The operation of the MCA was

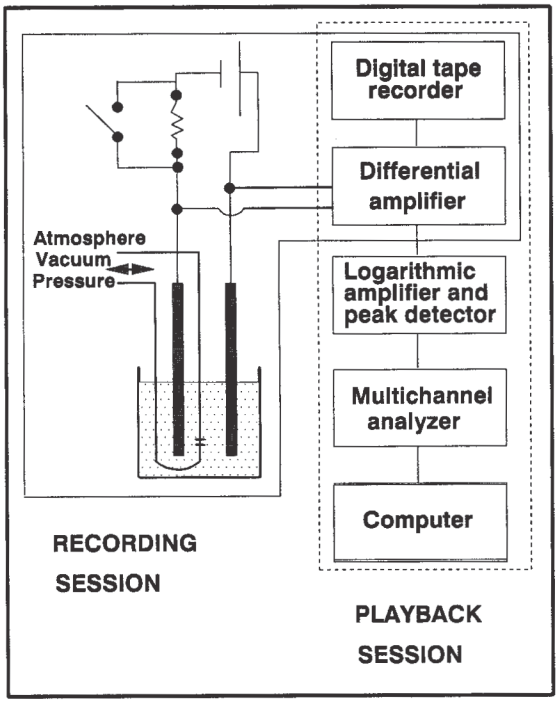

Figure 9. A schematic of LIMCA apparatus

controlled by connecting the MCA to a PC. Conversion of the voltage pulses to particle size distribution was performed through a LIMCA software package.

II.2.c. Experimental Procedure:

Figure 10. shows the experimental procedure followed during the LIMCA experiments.

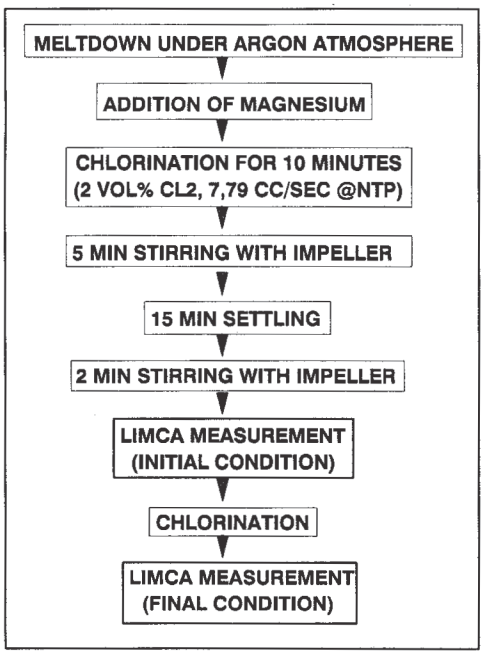

Figure 10. Experimental procedure followed for the LIMCA experiments.

The charge was first melted under an argon atmosphere. Following the addition of magnesium, the melt was injected with a 2% Cl_2-Argon gas mixture for 10 minutes while stirred by the impeller. After injection of the chlorine, the melt was stirred by the impeller for 5 minutes. Then, the impeller was stopped and the melt was allowed to settle for 15 minutes. Following this, the melt was stirred 2 minutes by the impeller and a first LIMCA measurement was taken. This represented the initial condition of the melt. Next, a mixture of chlorine and argon was injected to give a fixed quantity of chlorine regardless of the gas flowrate and chlorine concentration used. Immediately following gas injection, a second LIMCA measurement was taken to represent the final particle distribution of the melt. The experimental schedule followed for the LIMCA tests is presented in Table 2. The tests were carried out only for aluminum-1wt% magnesium alloys. Three different gas flowrates and chlorine concentrations were employed at 730 ^{0}C.

Table 2. Schedule followed for the LIMCA experiments

GAS FLOWRATE (CC/SEC) @NTP	VOL% CL2
	AL-1WT% MG
7.79	2
	10
	25
16.77	10
27.07	10

III. RESULTS AND DISCUSSIONS:

The experimental results were first tested for stoichiometric removal of sodium from the melt according to Equation 6. The results are shown in Figures 11a to f. As seen for both commercially pure aluminum and aluminum-1 wt% magnesium alloy experimental points lie below the theoretical 45^0 dotted line. The theoretical line was most closely approached when the chlorine concentration inside the gas bubbles was at a minimum.

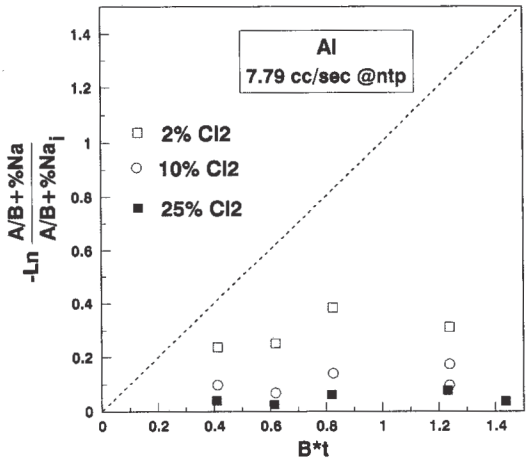

a

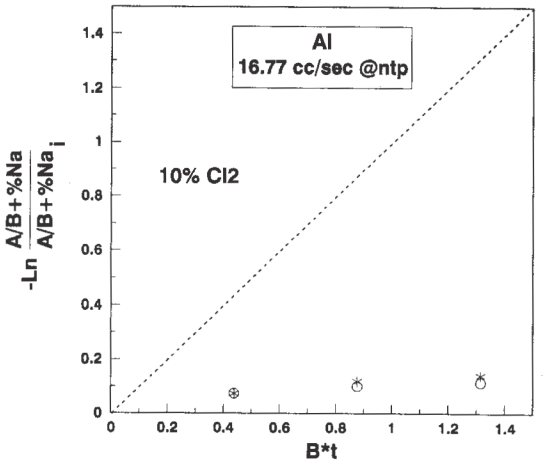

b

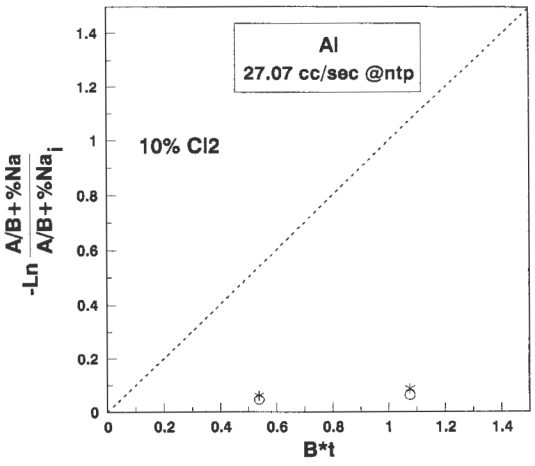

c

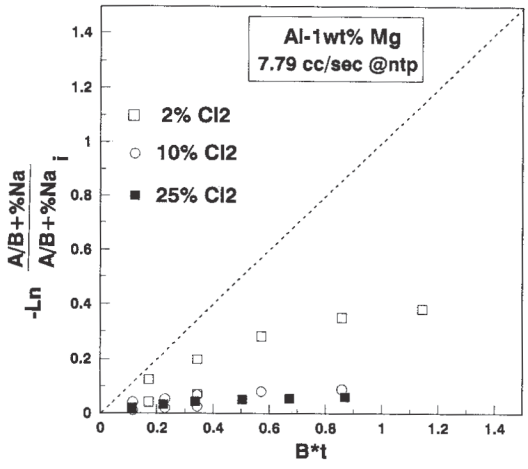

d

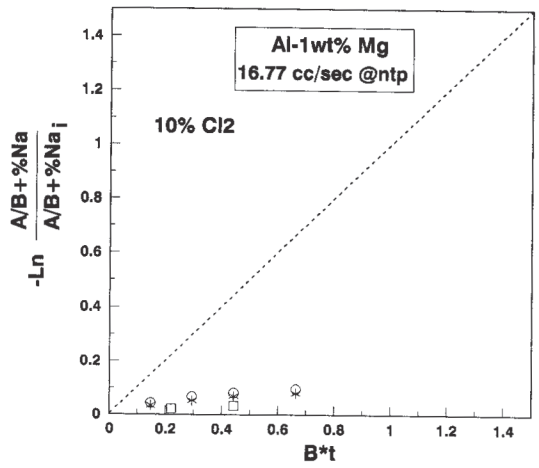

e

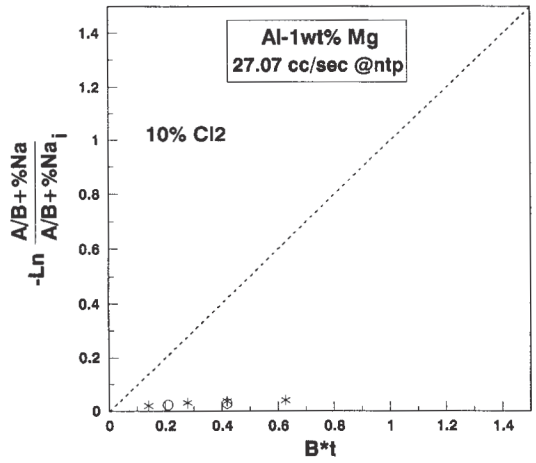

f

Figure 11. Comparison of theory and experimental results according to Equation 6.

The departure from the theoretical line became more pronounced with increase in chlorine concentration and gas flowrate.

These results show that under the present experimental conditions the stoichiometric removal of sodium with chlorine did not take place. In other words, the bubble-metal surface area and/or residence time of the bubbles were insufficient to consume all the chlorine within the Ar-Cl_2 gas bubbles.

These results suggest that under present experimental conditions, the removal of sodium was limited by the transport of sodium to the bubble-metal interface. Therefore, the kinetic model for mass transfer controlled sodium removal can apply.

In the following, the individual rate constants in Equation 1., that were obtained experimentally will be presented and results will be discussed. Individual rate constants were obtained from the slope of the straight lines that resulted from plotting $\ln(Na_t/Na_i)$ vs time.

For the evaporation term, the individual rate constant was obtained from the following relationship:

$$\frac{\%Na_t}{\%Na_i} = -\exp\left(\frac{G_{ar}\ K\ f_{Na}\ 100\ m_{Na}}{M\ P_{atm}} + \frac{k_0\ A_0\ \rho}{M}\right) t \qquad (9)$$

The first term on the right side gives the rate of removal of sodium through saturation of the gas bubbles with sodium vapour. This value was calculated and subtracted from the overall rate constant which was obtained from argon injection experiments to give the individual rate constant for evaporation from surface i.e the second term in the parentheses.

The individual rate constant for the chloride phase was obtained from the results of the intermittent tests according to the following equation:

$$\frac{\%Na_t}{\%Na_i} = -\exp\left(\frac{G_{ar}\ K\ f_{Na}\ 100\ m_{Na}}{M\ P_{atm}} + \frac{k_0\ A_0\ \rho}{M} + \frac{k_d\ A_d\ \rho}{M}\right) t \qquad (10)$$

The third term in the parentheses which is the rate constant for the chloride phase was obtained by subtracting the first two terms, which were obtained from separate argon injection experiments, from the overall rate constant obtained from the intermittent tests.

Rate constants for the bubbles were obtained by subtracting individual rate constants for evaporation and droplets from the overall rate constant which was obtained after the chlorination experiments according to Equation 1.

Figure 12. shows overall rate constants for argon injection tests for three different gas flowrates at 730 ^{0}C. As seen in the case of commercially pure aluminum, the removal of sodium was much faster than in aluminum-1 wt% alloy.

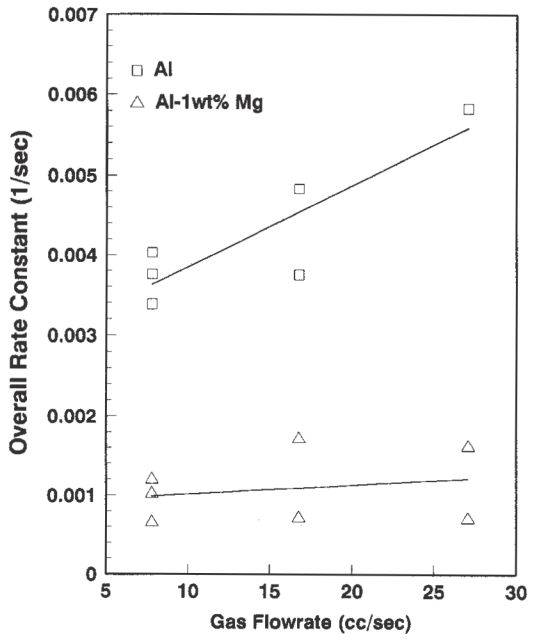

Figure 12. Overall rate constants as a function of gas flowrate(@NTP) obtained after argon gas injection

The difference between the removal rates was surprisingly large. This may be due to the permeability of MgO or Al_2O_3MgO spinel to sodium or decrease in the diffusion coefficient of sodium with the addition of magnesium into the melt.

Figure 13. shows overall rate constants that correspond to chlorination experiments and rate constants for the chloride phase as a function of chlorine concentration at 730 ^{0}C.

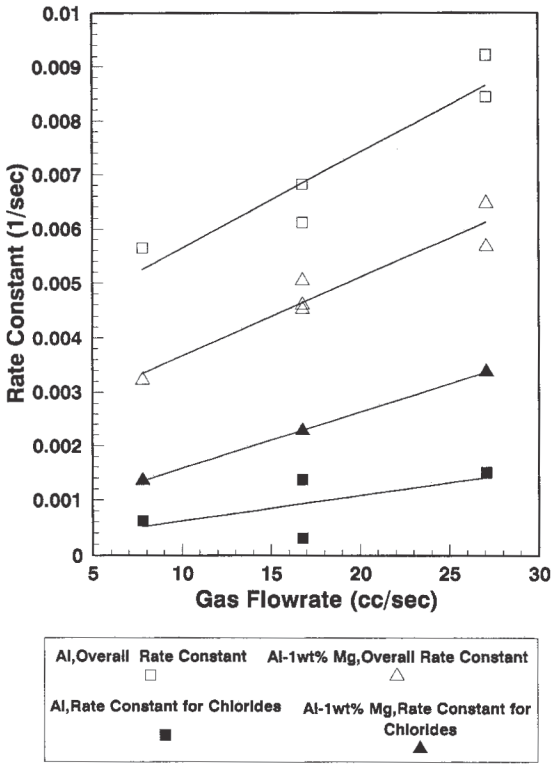

Figure 13. Overall rate constants for chlorination experiments and rate constants for the chloride phase as a function of Cl_2 concentration at 730 ^{0}C and at a gas flowrate of 7.79 cc/sec(@NTP)

It can be seen that the rate of removal of sodium from commercially pure aluminum was almost twice as fast than that from aluminum-1wt% magnesium alloy. It is also seen that the chloride phase contributed to the overall rate constant by about 40 % and 10 % for 1wt% magnesium alloy and commercially pure aluminum respectively.

Figure 14. shows mass transfer coefficients for the bubbles as a function of chlorine concentration in the bubbles at a gas flowrate of 7.79 cc/sec(@NTP) at 730 ^{0}C. Mass transfer coefficients were calculated from individual rate constants for the bubbles. Since the bubble frequency was measured during the experiments, the surface area of the bubbles at any instant in the bath was calculated assuming that the bubbles were spherical in shape. The bubble surface area of the bubbles at any instant in the bath was calculated from:

$$A_b = \frac{6\ Q\ h}{U\ d} \qquad (11)$$

Rising velocity of the bubbles was calculated from[6]:

$$U = 1.02 \left(\frac{g\ d}{2}\right)^{0.5} \qquad (12)$$

Table 3. shows typical bubble frequencies and the equivalent diameter of a single gas bubble at a corresponding gas flowrate.

Table 3. Typical bubble frequencies and corresponding bubble sizes @ 730 °C

GAS FLOWRATE (CC/SEC) @730 °C	BUBBLE FREQUENCY (1/SEC)	BUBBLE DIAMETER (CM)
26.2	13	1.56
56.45	16	1.89
91.12	16	2.22

It is seen in Figure 14. that the value of the mass transfer coefficients for bubbles inside the commercially pure aluminum was about twice that of mass transfer coefficients in the 1wt% magnesium alloy.

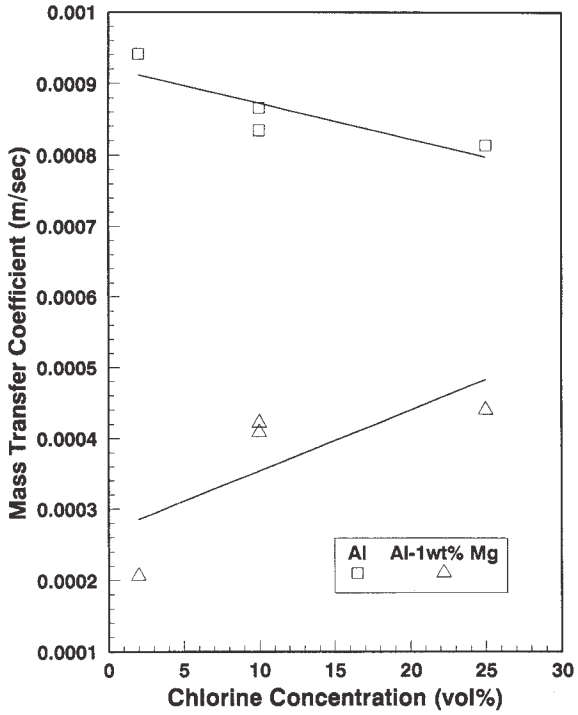

Figure 14. Mass transfer coefficients as a function of Cl_2 concentration at 730 °C and at a gas flowrate of 7.79 cc/sec(@NTP)

At this point, it is useful to compare the liquid phase mass transfer coefficients with the values based on Higbie's penetration theory[7]. According to the penetration theory the liquid phase mass transfer coefficient is given by:

$$k_L = 2 \left(\frac{D}{\pi\ \tau}\right)^{0.5} \qquad (13)$$

If one takes the D as 10^{-8} m^2/sec, the mass transfer coefficient for a bubble of $1.6*10^{-2}$ m equivalent diameter becomes $0.476*10^{-3}$ m/sec. This value is close to the mass transfer coefficient obtained experimentally in aluminum-1wt% magnesium alloy. However, it is half the value obtained for the commercially pure aluminum. In the case of commercially pure aluminum, the mass transfer coefficients obtained experimentally could be matched with predictions based on the penetration theory only if the diffusion coefficient of sodium is taken to be in the order of 2.5 to $3*10^{-8}$ m^2/sec.

Figure 15. shows the overall rate constants and the rate constants for the chloride phase as a function of gas flowrate at 730 °C. As seen, the rate constants increased with increase in gas flowrate. The contribution from the chloride phase to the overall reaction rate constant increased from 40 to 60% for the magnesium alloy and from 10 to 25% for the commercially pure aluminum.

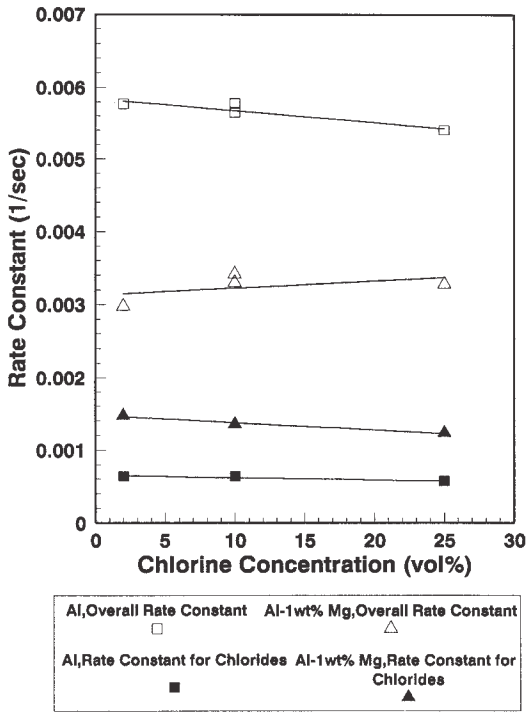

Figure 15. Overall rate constants and rate constants for the chloride phase as a function of gas flowrate(@NTP) at 730 °C

Figure 16. shows mass transfer coefficient for the bubbles as a function of gas flowrate at 730 °C. In the case of the magnesium alloy, the value of the mass transfer coefficient was 2 to 3 times smaller and mass transfer coefficients decreased with increase in the gas flowrate due to the increased bubble sizes.

In the evaluation of the LIMCA data, the amount of the $MgCl_2$ droplets that were generated by the bubbling action of chlorine was taken to be the difference between the counts right after the bubbling and the initial count.

Figure 17. shows the number of particles that was greater than 22 micrometer diameter per 7.5 kg of melt as a function of chlorine concentration and flowrate (@ NTP) employed. As seen, as the chlorine concentration and gas flowrate increased, the difference between the initial count and the count immediately after chlorine bubbling increased. One can therefore postulate that more and more $MgCl_2$ droplets

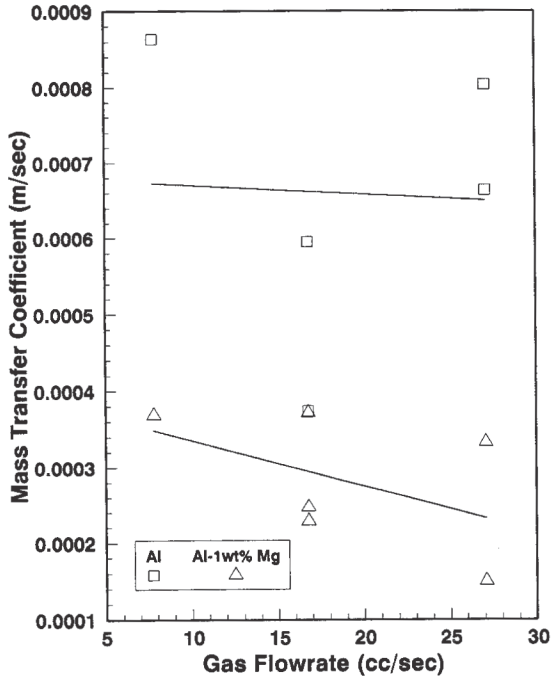

Figure 16. Mass transfer coefficients for the bubbles as a function of gas flowrate(@NTP) at 730 ^{0}C

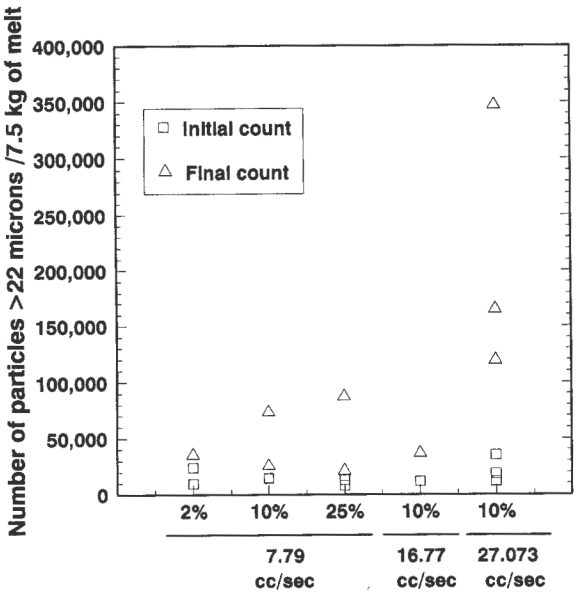

Figure 17. Number of particles as a function of Cl_2 concentration and gas flowrate(@NTP)

became present inside the melt with increase in chlorine concentration and gas flowrate.

To show the implication of this data lets consider the case where the gas flowrate was 27.07 cc/sec (@ NTP) and chlorine volume fraction was 10 %. The data that corresponds to this case is presented in Figure 18.. First the difference in the number of counts was calculated. From this, area of the

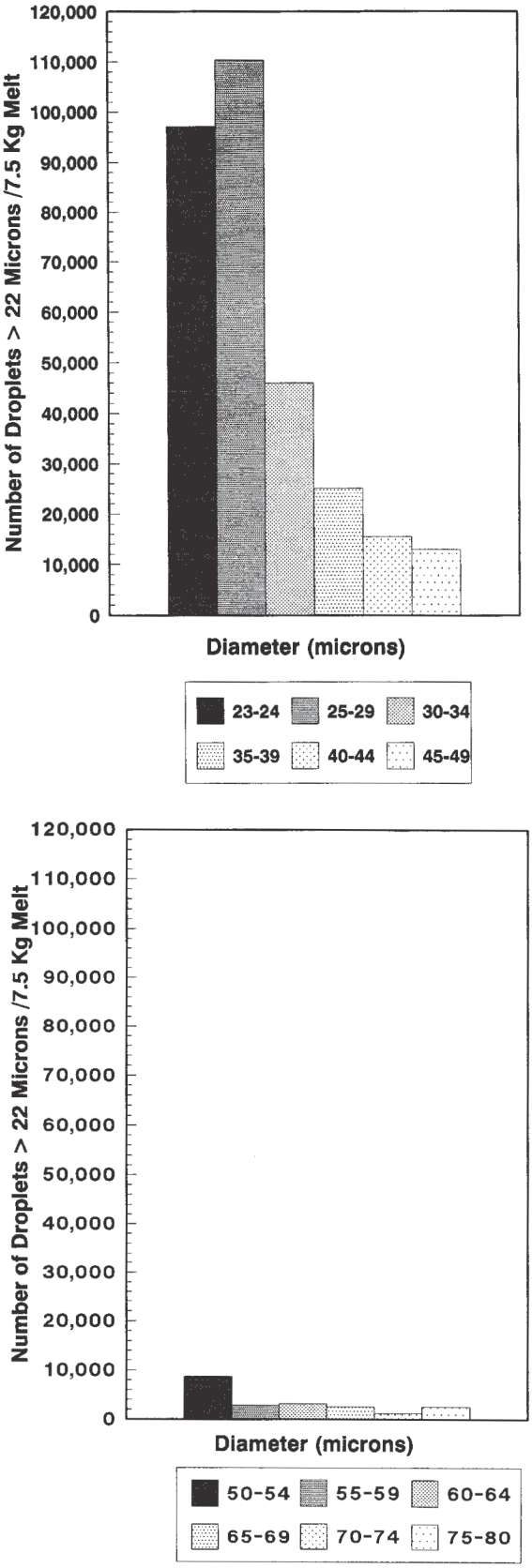

Figure 18. Droplet size distribution at 27.07 cc/sec gas flowrate(@NTP) and 10% Cl_2 concentration.

droplets was calculated to be $1.09846*10^{-3}$ m^2 assuming that they were spherical in shape. Inserting this number into an experimentally determined individual rate constant corresponding to this gas flowrate and chlorine concentration which was obtained after the intermittent test one obtains:

$$\frac{k_d \; 1.09846*10^{-3} \; 2360}{7.5} = 0.00345 \qquad (14)$$

$k_d = 1*10^{-2}$ m/sec. In this equation D was taken to be 10^{-8} m^2/sec. This value was at least an order of magnitude greater than expected even if all the droplets were 20 micrometer in diameter according to the relation[7]:

$$Sh = \frac{k_d \, d_d}{D} = 2 \qquad (15)$$

This equation is valid for droplets carried along with the fluid i.e having no relative velocity with respect to the fluid that they are in. Since $MgCl_2$ droplets have almost the same density as the melt itself(2300 vs 2360 kg/m^3), Equation 15. should represent the process under consideration. Since k_d can not be this big a number, the rate constant originally postulated for droplets can not be represented only by the droplets inside the melt. We therefore postulate that only a portion of the rate constant for the chloride phase can be represented by the droplets. The rest must presumably come from the amount of $MgCl_2$ salt carried to the crucible walls and covering various parts. To calculate the contribution to the chloride rate constant by droplets, Equation 15. was used together with the experimental LIMCA data to find first an average semi-empirical mass transfer coefficient for the droplets according to :

$$k = \frac{\sum k_d A_d}{\sum A_d} \qquad (16)$$

Semi-empirical rate constants thereby obtained for the chloride droplets were compared with the rate constants obtained from the intermittent tests. The results of these calculations are shown in Figure 19.. As seen the contribution of the droplets to the total rate changed between 1 to 7% only.

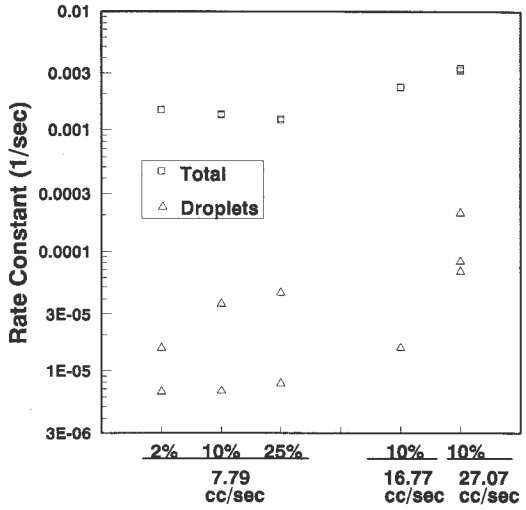

Figure 19. Overall rate constants for the chloride phase and rate constants for the droplets as a function of Cl_2 concentration and gas flowrate(@NTP)

X-ray diffraction analyses of the dross samples showed that in the case of the magnesium alloy, $MgCl_26H_2O$ was present together with the spinel. However, in case of the commercially pure aluminum only Al_2O_3 could be detected. No chloride phase could be detected possibly because of the relatively small amount of chloride making elements in the commercially pure aluminum melt.

IV. CONCLUSIONS:

1) Under the present experimental conditions, the removal of sodium from commercially pure aluminum and aluminum-1wt% magnesium alloy was controlled by the transport of sodium in a liquid phase mass boundary layer.

2) Liquid phase mass transfer coefficients calculated for the bubbles suggests that the value of the diffusion coefficient of sodium in aluminum-1wt% magnesium alloy should be about three times smaller than its value in commercially pure aluminum. However, this has yet to be proved by theoretical calculations.

3) In case of aluminum-1wt% magnesium alloy, intermediate reaction products($MgCl_2$) played an important role in the removal of sodium. Calculations showed that intermediate reaction products in the form of droplets inside the melt contributed only negligibly to the overall reaction rate. Therefore it was postulated that most of the intermediate reaction products should deposit on the crucible walls that acted as a further reaction site for sodium.

List of Symbols:

A Surface area (m^2)
D Diffusion coefficient (m^2/sec)
d Diameter (m)
f Frequency of bubble formation (1/sec)
f_{Na} Activity coefficient of Na
g Gravitational acceleration (m/sec^2)
h Height of the metal column (m)
K Equilibrium constant
k Mass transfer coefficient (m/sec)
M Metal weight (kg)
m Molecular weight (kg/k-mole)
Q Gas flowrate (k-mole/sec)
Sh Sherwood number
U Bubble rise velocity (m/sec)

Greek symbols:

Y Electrical resistivity of the melt (ohm-m)
ρ Density of the melt (kg/m^3)
τ Sweep time across the bubble surface calculated according to the bubble diameter (sec)

Superscripts:

b bubble
d chloride droplets
o evaporation

Subscripts:

ar argon gas
b bubble
Cl_2 chlorine gas
d chloride droplets
I interfacial
i initial
L liquid
o evaporation
t transient

ACKNOWLEDGMENTS

The authors acknowledge helpful discussions with Dr. D. Doutre of Alcan Int. Ltd., Kingston during the course of this study; Alcan Int. Ltd., Kingston for making their facilities available for the analysis of the samples; Mr. D. Choquette of Alcan Int. Ltd., Arvida for supervising the chemical analyses of the samples; NSERC for the financial support for B. Kulunk.

REFERENCES:

1. S. Kaestner, J. Krueger, F. Patak, "Refining of Virgin Aluminum by Scavenging Gas Treatment", Raffinationsverfahren Metall., Int. Symp., 1983, 36-53

2. O. Hjelle, T.A. Engh, B. Rasch, "Removal of Sodium from Aluminum-Magnesium Alloys by Purging with Argon and Cl_2", Refining and Alloying of Liquid Aluminum and Ferroalloys, [Proc. Conf], The Norwegian Institute of Technology, Torondheim, Norway, Aug 1985, 343-360

3. J.J. Mitchell, C.S. Samis, "Activity of Sodium in the Na-Al System and NaF and AlF_3 Activities in $NaF.AlF_3$ Melts", Transactions of the Metallurgical Society of AIME, 245, (June 1969), 1227-1234

4. R. Hultgren et al., Selected Values of Thermodynamic Properties of Metals and Alloys, April 1958, 417-422

5. D. Doutre, "The Development and Application of a Rapid Method of Evaluating Molten Metal Cleanliness", (Ph.D. Thesis, McGill University, 1984

6. J. Botor, "Mass Transfer Surface in the Process of Liquid Metal Bubbling", Metallurgia I Odlewnictwo, (1981), 393-406

7. R. Higbie, "The Rate of Absorbtion of a Pure Gas into a Still Liquid During Short Periods of Exposure", Transactions of the American Institute of Chemical Engineers, 31, (1934-35), 365-388

8. W.E Ranz, W.R Marshall, "Evaporation from Drops, Part I", Chemical Engineering Progress, 48, (3), (March 1952), 141-146